Electronics and Electrical Engineering

http://www.aimspress.com/journal/ElectrEng

AIMS Electronics and Electrical Engineering, 7(4): 231–242.
DOI: 10.3934/electreng.2023014
Received: 16 August 2023
Revised: 23 September 2023
Accepted: 10 October 2023
Published: 16 October 2023

Research article

A low-loss dual-band bandpass filter using open-loop stepped-impedance resonators and spur-lines for sub-6 GHz 5G mobile communications

Rachida Boufouss*and Abdellah Najid

Department of Communication Systems, National Institute of Posts and Telecommunications, Madinat Al Irfane, 10112 Rabat, Morocco

* **Correspondence:** Email: boufouss.rachida@gmail.com.

Abstract: This article presents the design of a low-loss microstrip dual-band bandpass filter with improved inter-band isolation and selectivity for 5G sub-6 GHz mobile communications. The proposed filter utilizes the two first resonance mode frequencies provided by the stepped-impedance resonator to generate its two passbands at 3.6 GHz and 3.5 GHz, and spur-lines located before the input/output ports to improve the isolation and selectivity between passbands. The filter is designed using an RT/Duroid 5870 substrate with a relative permittivity of 2.33 and a thickness of 0.79 mm, manufactured and tested to validate the proposed design. The experimental results show that the filter operates at 3.61 GHz and 5.51 GHz with a 3-dB fractional bandwidth of 12.74% and 16.7%, respectively. Insertion losses at the two passbands center frequencies are 0.6 dB and 0.9 dB. In addition, the proposed filter has the advantage of covering the licensed and unlicensed 5G bands and provides a simple structure without using vias or DGS structures.

Keywords: 5G; bandpass filter; dual-band; stepped-impedance resonator; spur-line; sub-6 GHz

1. Introduction

The sub-6 GHz spectrum is getting more congested with several applications. Given that the licensed 5G bands may not have sufficient bandwidth to fulfill 5G requirements in this spectrum, the unlicensed band 5150–5925 MHz has recently been included in the 5G spectrum to satisfy high data rate requirements. Therefore, low-loss, compact dual-band bandpass filters (BPFs) with good passband selectivity and high inter-band isolation are highly demanded for 5G mobile communications.

In recent years, a large variety of different methods have been developed and utilized to design dual-band BPFs, such as combining two single-band BPFs with different passbands. For instance, by using open-circuited stubs [1] and sub-loaded open complementary split-ring resonator (SL-OCSRR) [2]. Or using the first two resonance frequency modes of loaded resonators [3] and stepped-impedance

resonators (SIRs) [4]. Furthermore, substrate-integrated waveguides have also been used to design widely separated passbands [5, 6]. Besides, several works and techniques have been reported in the literature to reduce the size of the filter. Among them, folding the two open-ended arms of SIR coupled with each other [7], bending microstrip lines, rectangular and SIR resonators [8], using $\lambda/4$ and multimode resonators [9–11].

For 5G mobile communications, various single- and dual-band BPFs have been reported in recent years [12–18]. In [12], a single-band CPW BPF is formed by using spiral-shaped DGSs and m-shaped DGSs. It resonates at 3.45 GHz with a fractional bandwidth of 10.1% ranging from 3.35 to 3.71 GHz. A wideband BPF with broad stopband and ultra-wide reflectionless range is reported in [13], where the measured operating frequency is from 3.1 to 5.3 GHz. A high selectivity narrowband SIW cavity BPF with perturbing vias and CSRR operating at 4.947 GHz with a fractional bandwidth of 1.16% is presented in [14]. Furthermore, a quasi-elliptic dual-band planar BPF centered at 4.6 GHz and 5.4 GHz is presented in [15], where the fractional bandwidth of the two passbands are 13.5/11.5%. A miniaturized dual-band filter using dual-mode dielectric waveguide resonator is studied in [16], it resonates at 2.91/3.53 GHz with a fractional bandwidth of 2.27/1.67%. A compact dual-band BPF based on the substrate integrated suspended line (SISL) platform that operates at 3.46/4.87 GHz with a fractional bandwidth of 16.2/7.7% is presented in [17]. A self-packaged dual-band BPF centered at 3.45/4.9 GHz with a fractional bandwidth of 11.0/6.9% is designed in [18]. However, all these reported filters work only in the licensed 5G bands.

This article presents several complementary improvements related to our previous work in [18], which aimed to design a compact dual-band BPF for the licensed 3400–3800 MHz and unlicensed 5150–5850 MHz 5G bands and discuss the results obtained from simulations and measurements. In addition to that, a comparison between the proposed dual-band BPF and other recent 5G BPFs is provided.

The organization of the rest of this article is as follows: Section 2 presents the details of the analysis and design procedure of the dual-band BPF. Then, simulated and experimental results are given in Section 3. Finally, conclusions are presented in Section 4.

2. Design and analysis of the proposed dual-band BPF

The design of the proposed dual-band BPF is accomplished by using two open-loop SIRs and two spur-lines fed by 50 Ω input/output tapped lines. In this work, all simulations have been carried out using CST Microwave Studio software.

2.1. Design of dual-band BPF using two open-loop SIRs

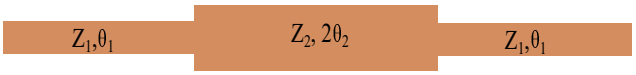

Figure 1. The conventional structure of the $\lambda_g/2$ SIR.

SIR is often utilized to design dual-band BPF. Its conventional structure is shown in Figure 1 consisting of a low-impedance section in the middle of characteristic impedance Z_2 and two high-impedance sections of characteristic impedance Z_1 at both sides. The electrical lengths of the low and

high impedance lines are $2\theta_2$ and θ_1, respectively. In our design, we chose $\theta_1 = \theta_2 = \theta$ for simplicity. In this case, the input impedance of the conventional SIR can be expressed as [20]:

$$Z_{in} = jZ_1 \frac{-R_Z(1 - \tan^2\theta) + 2(1 + R_Z^2)\tan^2\theta}{2\tan\theta(R_Z + 1)(R_Z - \tan^2\theta)}. \tag{2.1}$$

where $R_z = Z_1/Z_2$ is the ratio of the two characteristic impedances. The resonance conditions, i.e., $Y_{in} = 1/Z_{in} = 0$, can be described by the two equations:

$$\begin{cases} R_Z - \tan^2\theta = 0 \\ \tan\theta = 0 \end{cases} \tag{2.2}$$

Thus, the first four resonant mode frequencies f_1, f_2, f_3 and f_4 can be deduced from Eq. 2.2, which can be expressed as

$$\theta(f_1) = \tan^{-1}\sqrt{R_Z} \tag{2.3}$$

$$\theta(f_2) = \frac{\pi}{2} \tag{2.4}$$

$$\theta(f_3) = \pi - \tan^{-1}\sqrt{R_Z} \tag{2.5}$$

$$\theta(f_4) = \pi. \tag{2.6}$$

Therefore, the normalized frequencies f_2/f_1, f_3/f_1 and f_4/f_1 can be written as

$$\frac{f_2}{f_1} = \frac{\theta(f_2)}{\theta(f_1)} = \frac{\pi}{2\tan^{-1}\sqrt{R_Z}} \tag{2.7}$$

$$\frac{f_3}{f_1} = \frac{\theta(f_3)}{\theta(f_1)} = \frac{\pi}{\tan^{-1}\sqrt{R_Z}} - 1 \tag{2.8}$$

$$\frac{f_4}{f_1} = \frac{\theta(f_4)}{\theta(f_1)} = \frac{\pi}{\tan^{-1}\sqrt{R_Z}}. \tag{2.9}$$

To design the dual-band BPF, the first and second resonant frequencies of the SIR f_1 and f_2 are used as the center frequencies of the upper and lower passband of the filter. In our study, we set f_1 = 3.6 GHz and f_2 = 5.5 GHz. According to equation (2.7), the calculated impedance ratio R_Z is 2.75. By choosing $Z_1 = 50\ \Omega$, the initial lengths and widths of the low and high impedance lines of the SIR can be calculated using the following formulas:

$$Z_0 = \frac{120\pi}{\sqrt{\epsilon_e}[W/h + 1.393 + 0.667\ln(W/4 + 1.444)]}, \tag{2.10}$$

$$\epsilon_e = \frac{\epsilon_r + 1}{2} + \frac{\epsilon_r - 1}{2}\frac{1}{\sqrt{1 + 12h/W}}, \tag{2.11}$$

$$\theta = \beta l, \tag{2.12}$$

$$\beta = \frac{2\pi}{\lambda_g}, \lambda_g = \frac{\lambda_0}{\sqrt{\epsilon_e}}. \tag{2.13}$$

where Z_0 is the characteristic impedance of the microstrip line, h is the thickness of the substrate, ϵ_r and ϵ_e are the relative and effective dielectric constants of the substrate and λ_g and λ_0 are the guided and free-space wavelengths, respectively. These initial parameters are: $L_1 = 9.76$ mm, $L_2 = 19.52$ mm, $w_1 = w_2 = 2.37$ mm, $w_3 = 0.24$ mm, $g_1 = 0.5$ mm and $g_2 = 0.6$ mm. For miniaturization, two open-loop SIRs are used rather than conventional SIRs fed by 50 Ω input/output tapped lines, as shown in Figure 2. The reason behind choosing the tapped lines to excite the filter is to produce two transmission zeros in the lower and upper stopband of the first passband [19]. The response of the filter is depicted in Figure 3, which illustrates that f_1 constructs the first passband at 3.78 GHz, whereas f_2 constructs the second passband at 5.87 GHz. Some slight discrepancies between analysis and simulation are observed due to the coupling between resonators and the coupling between the edges of the high-impedance lines, since in the analysis one SRR is considered. This deviation can be fixed by varying the length of the SIR.

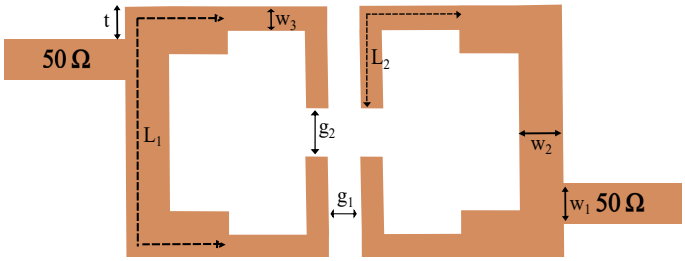

Figure 2. Structure of the dual-band BPF.

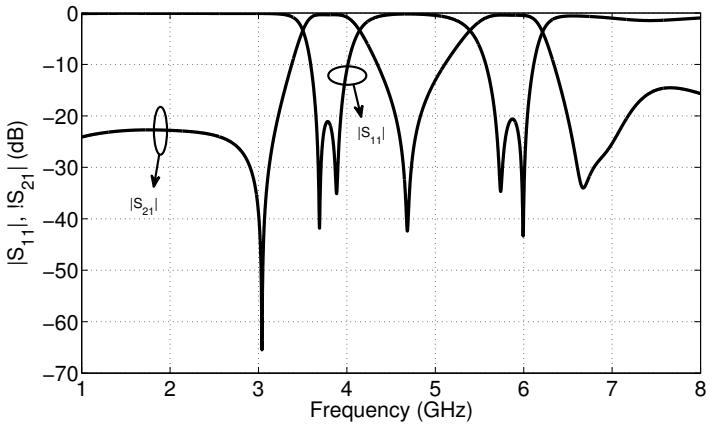

Figure 3. Simulated response of the initial-designed bandpass filter.

From Figure 4, it can be seen that the bandwidth of the first passband is affected by the position of the tapped line. As the tapping position becomes closer to the center position of the resonator, the external quality factor value becomes larger since the bandwidth becomes narrower. Plus, the bandwidth of both passbands can also be simultaneously adjusted by properly changing the separation between resonators g_1 as illustrated in Figure 5. The smaller is the separation, the larger is the bandwidth.

As the tapped lines produce two transmission zeros in the lower stopband of the first passband and between two passbands, another transmission zero can be observed in the upper stopband of the filter.

This transmission zero can be adjusted by controlling the coupling between high-impedance lines, as shown in Figure 6. By selecting the appropriate value of the gap, g_2, the out-of band rejection and the skirt characteristic of the upper band-edge of the second passband can be improved.

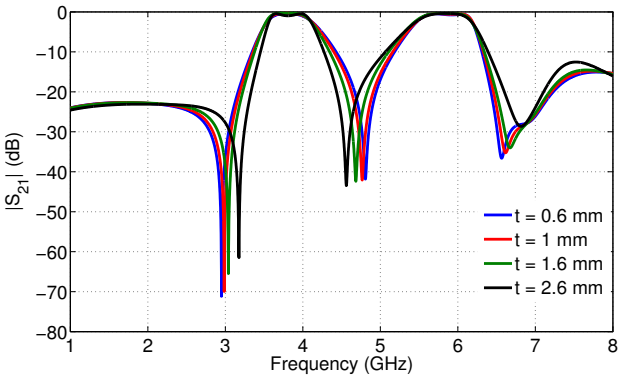

Figure 4. Variation of $|S_{21}|$ versus the tapped feeding lines t.

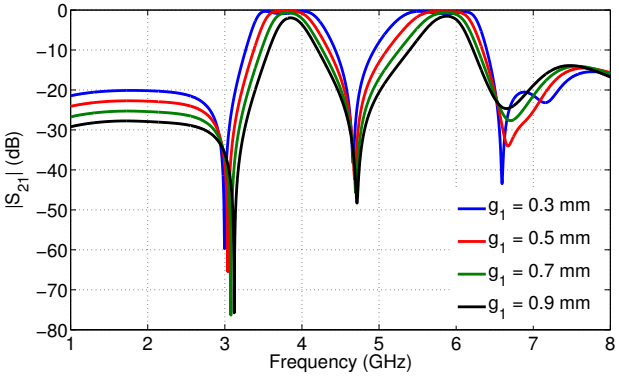

Figure 5. Variation of $|S_{21}|$ versus the separation between resonators g_1.

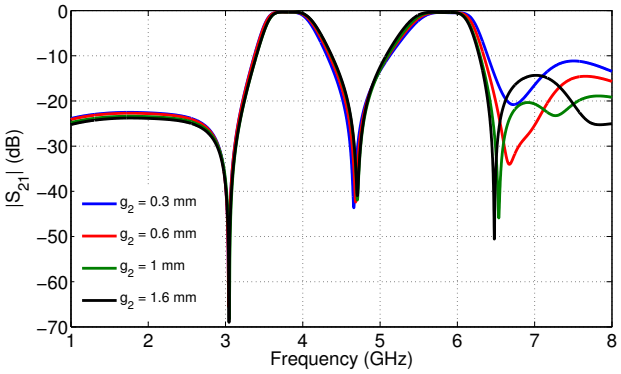

Figure 6. Variation of $|S_{21}|$ versus the gap between edges of the high-impedance lines g_2.

Based on this analysis, the filter above is optimized, and its final physical dimensions are as follows: $L_1 = 10.31$ mm, $L_2 = 20.65$ mm, $w_1 = w_2 = 2.37$ mm, $w_3 = 0.24$ mm, $g_1 = 0.58$ mm and $g_2 = 0.57$ mm. Figure 7 depicts its simulated frequency responses. As can be seen, the filter operates at 3.6 GHz and 5.55 GHz, covering 3381-3871 MHz and 8150-5840 MHz bands. Insertion losses of 0.37 dB at 3.6 GHz and 0.42 dB at 5.5 GHz with more than 26 dB and 30 dB return losses, respectively, were

achieved. Two transmission zeros in the lower and upper stopbands are clearly observed at 2.93 GHz and 6.29 GHz, and one transmission zero located at 4.4 GHz provides 43.6 dB isolation between passbands. Moreover, the roll-off rate of the lower transition of the upper passband is 49.4 dB/GHz. The size of the filter without feed lines is $0.25\lambda_g \times 0.30\lambda_g$, where λ_g is the guided wavelength at 3.6 GHz.

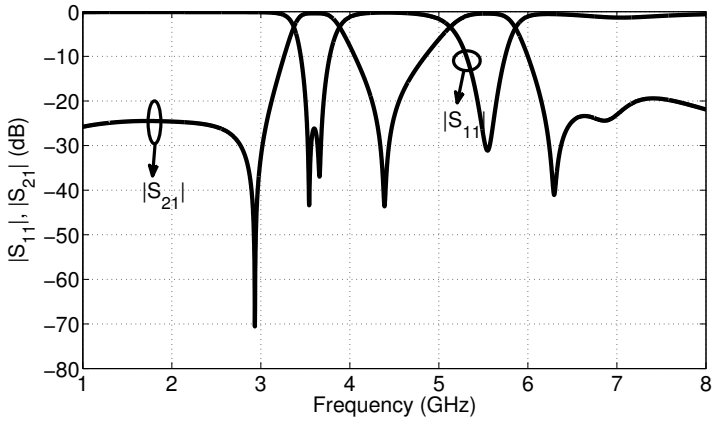

Figure 7. Simulated S-parameters of the filter shown in Fig. 2.

2.2. Inter-Band isolation and selectivity improvement

It is true that the passband frequencies of the filter can be controlled by the impedance ratio of the SIR. However, the inter-band isolation and selectivity of the filter must be improved, especially if the passband frequencies are widely separated. In our design, the two passbands are relatively close to each other. Adding a transmission zero between passbands should not affect the filter response. For that, to achieve the best performance with fabrication simplicity and low-cost methodology, a simple method based on adding a pair of spur-lines before the input/output ports of the filter is employed.

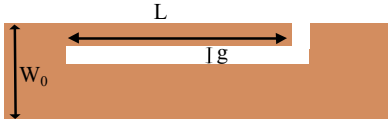

Figure 8. Structure of the spur-line section.

In general, the spur-line can be created by etching an L-slot in the main transmission line, as depicted in Figure 8, where W_0 and L are the width of the main transmission line and the length of the spur-line, which is equal to the quarter-wavelength at the fundamental frequency. g is the gap between the coupled lines. Figure 9 depicts the structure of the improved filter. Here, the spur-lines are meandered to reduce the size of the filter. Based on the results shown in Figure 7, the variation of the introduced transmission zero is investigated when the length of the spur-line is varied (Figure 10). As can be seen, the frequency of the transmission zero increases with increasing length L. Also, it can be anticipated from Figure 11 that the two transmissions zero between passbands become insensitive to the gap g when its value becomes larger. In this case, the two transmission zeros can be overlapped.

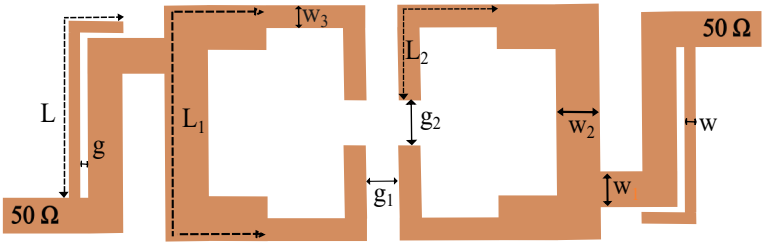

Figure 9. Structure of the improved dual-band BPF.

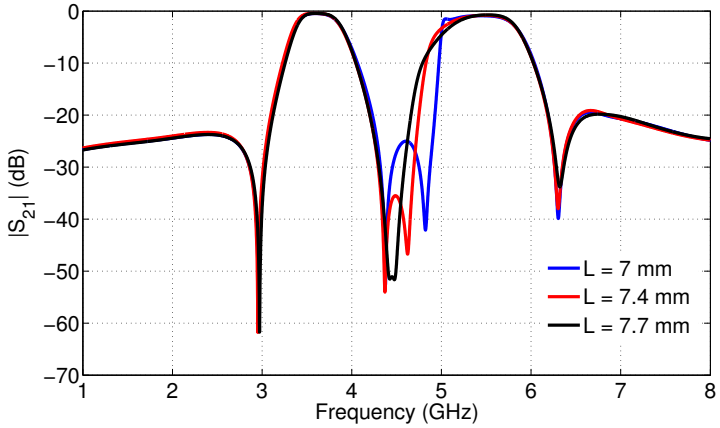

Figure 10. Variation of $|S_{21}|$ versus the length of the spur-line L.

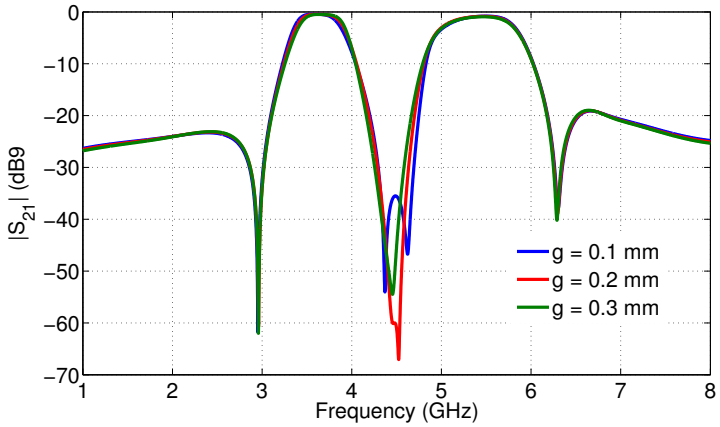

Figure 11. Variation of $|S_{21}|$ versus the gap of the spur-line g.

Figure 12 shows the simulated frequency responses for the filter with and without spur-line, it is found that the transmission zero, which is caused by adding the spur-line, has improved the isolation between the two passbands (48.2 dB) and also the selectivity of the second passband (the roll-of rate of the lower transition of the upper passband is 69.2 dB/GHz) without perturbing the response of the previous filter.

The current distributions of the proposed dual-band BPF filter at the center frequencies 3.6 GHz and 5.5 GHz and at the transmission zero frequencies 2.95 GHz, 4.4 GHz, 4.5 GHz and 6.3 GHz are

shown in Figure 13. From this figure, we can observe that high current is concentrated on the high impedance lines at 3.6 GHz and 5.5 GHz. However, there is no current flowing from the input port to the output port at 2.95 GHz, 4.4 GHz, 4.5 GHz and 6.3 GHz, which indicates the BPF behavior of the structure.

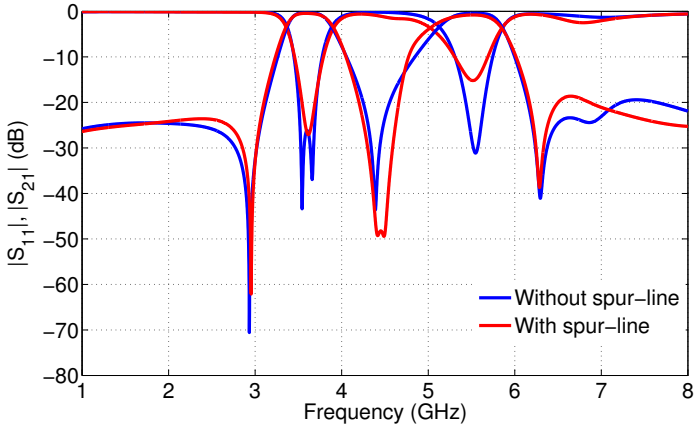

Figure 12. Comparison between the filter with and without spur-line.

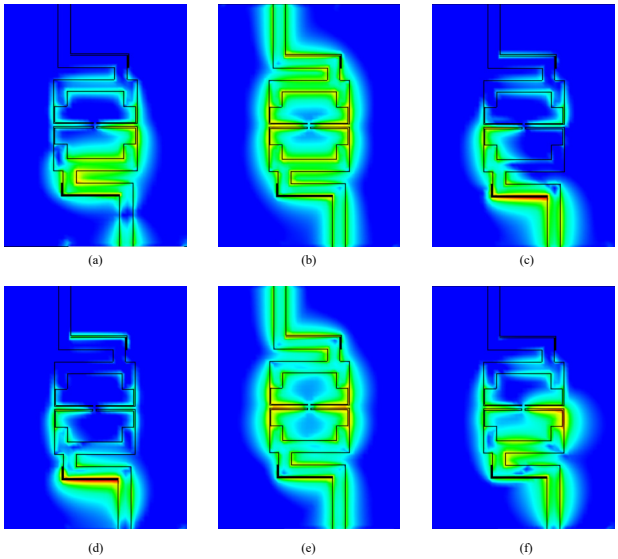

Figure 13. Simulated current distribution of the proposed dual-band BPF: (a) at 2.95 GHz, (b) at 3.6 GHz, (c) at 4.4 GHz, (d) at 4.5 GHz, (e) at 5.5 GHz and (f) at 6.3 GHz.

3. Experimental results and discussion

In order to examine the validity of the proposed design, the proposed dual-band BPF is designed and manufactured on an RT/duroid 5870 substrate with a relative permittivity of 2.33 and a thickness of 0.79 mm. Its physical dimensions are as follows: $L_1 = 20.65$ mm, $L_2 = 10.31$ mm, $w_1 = w_2 = 2.37$ mm, $w_3 = 0.24$ mm, $g = 0.1$ mm, $g_1 = 0.58$ mm, $g_2 = 0.57$ mm, $w = 0.2$ mm and $L = 13$ mm.

The photograph of the fabricated dual-band BPF with its measurement equipment are depicted in

Figure 14, and its size without feed lines is 0.25 $\lambda_g \times 0.47\lambda_g$, where λ_g is the guided wavelength at 3.6 GHz. Figure 15 depicts the simulated and measured S-parameters of the experimental filter designed at 3.6/5.5 GHz, and good agreement between them is observed. The measured center frequencies of the proposed dual-band BPF are 3.61 GHz and 5.51 GHz, with 3-dB bandwidth ranging from 3390 to 3850 MHz and 4970 to 5860 MHz, respectively. The measured in-band return losses are 32 dB and 17.2 dB, with insertion losses of 0.6 dB and 0.9 dB at 3.61 GHz and 5.51 GHz, respectively. Four measured transmission zeros are found at 2.94 GHz, 4.37 GHz, 4.58 GHz and 6.27 GHz with a peak attenuation of 40.4 dB, 48.6 dB, 45.8 dB and 39.3 dB, among them two between passbands. In addition to that, the out-of-band rejection in the lower stopband is better than 20 dB in the frequency range of 1 to 3.1 GHz, while in the upper stopband is better than 18 dB. The measured roll-off rate of the lower transition of the second passband is 101.6 dB/GHz.

Figure 14. Photograph of the fabricated dual-band BPF with its measurement equipment.

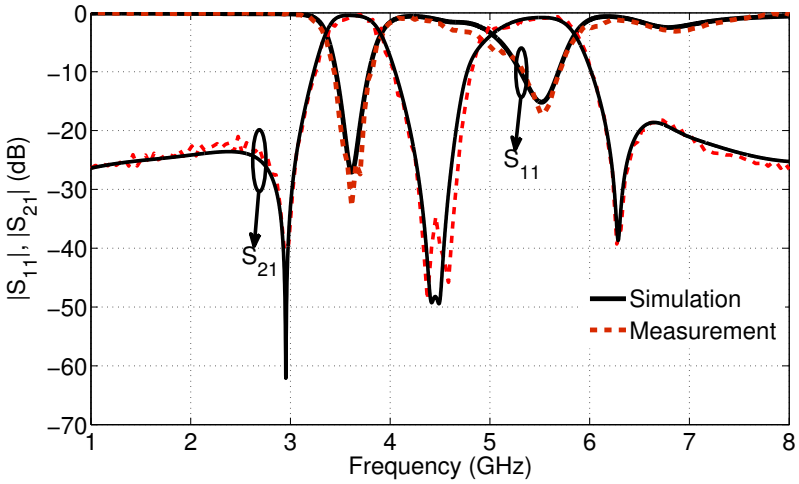

Figure 15. Simulated and measured S-parameters of the proposed dual-band BPF.

To highlight the performances of the proposed dual-band BPF, a comparison with other works are listed in Table 1. The benefits of our proposed filter can be summarized as follows: first, the proposed filter covers the licensed and unlicensed 5G bands. Second, the inter-band isolation and selectivity of the filter are improved due to the use of spur-lines before the input/output ports, which generate a transmission zero between passbands without degrading the passband performance. Finally, there is good performance in terms of low insertion loss, good return losses and simplicity of the design since no vias or DGS structures are used in this filter.

Table 1. Comparison between this work and other previous 5G BPFs.

Ref.	CFs (GHz)	FBW (%)	IL (dB)	RL (dB)	TZs	Out of-band rejection (dB)	Size ($\lambda_g \times \lambda_g$)
[12]	3.54	10.1	1.23	28.9	2	>20 (4.29-7 GHz)	0.42×0.37
[13]	4.2	52.4	1	-	-	30(6.5 f_0)	0.45×0.33
[14]	4.947	1.16	2.9	-	-	-	-
[15]	4.60 / 5.40	13.5 / 11.5	1.02/0.8	>20	3	>20 (5.7-8.8 GHz)	-
[16]	2.91/3.53	2.27/1.67	1/1.5	17/18	2	>20	0.18×0.17
[17]	3.46/4.87	16.23/7.70	4.36/5.77	-	-	15.2 (4.4f_0).	0.18×0.14
[21]	11.0/6.9	0.85/1.13	4.36/5.77	-	6	-	0.32×0.45
[22].B	2.66/3.54	7.89/4.52	0.86/1.53	> 18/> 15.4	2	> 20 (3.8-4.2 GHz)	0.122×0.22
[22].B	2.82/3.73	6.38/3.84	0.76/1.93	> 13.5/> 20	2	16 (3.88-5 GHz)	0.34×0.24
[22].C	2.84/3.74	5.98/3.47	1.72/2.02	> 12.4/> 17	2	16 (3.88-5)	0.34×0.24
[23]	3.45/4.9	7.82/4.08	1.15/1.42	–	5	-	0.21×0.31
[24]	0.946/1.48	9.8/9.5	2.16/1.26	> 10/ > 10	3	11.37 (1.6-2 GHz)	0.25×0.12
[25]	2.13/3.47	14/11.2	0.73/0.9	> 32/33	4	20 (3.85 -7.39 GHz)	0.214×0.22
This work	3.61/5.51	12.74/16.7	0.6/0.9	32.9/17.24	4	18(6.14-8 GHz)	0.25×0.47

4. Conclusions

This article presents a low-cost dual-band BPF using open-loop SIRs with improved inter-band isolation and selectivity centered at 3.61/5.51 GHz for 5G sub-6 GHz licensed and unlicensed bands mobile communications. Both simulation and measured results have been provided to validate the proposed design, and good agreement between them has been found. The transmission zero generated by the spur-line improves the isolation and selectivity between the closely spaced passbands without degrading the passband performance, making the filter easy to design and implement since no vias or DGS structures are used. The proposed dual-band BPF has insertion losses of 0.6 dB and 0.9 dB and return losses of 32.9 dB and 17.24 dB at 3.61 GHz and 5.51 GHz, respectively. The roll-off rate of the lower transition of the second passband is 101.6 dB/GHz, and the upper stopband ranges from 6.14 GHz to 8 GHz with a rejection level of 18 dB. Compared with other reported works, the proposed dual-band BPF exhibits the advantages of low insertion loss, good return loss and a simple structure, indicating that it would be a good candidate for 5G sub-6 GHz mobile communications.

Use of AI tools declaration

The authors declare they have not used Artificial Intelligence (AI) tools in the creation of this article.

Acknowledgments

The authors are grateful to Departamento de Ingenieria de Comunicaciones (DICOM), University of Cantabria (UNICAN), Spain, for support with regard to simulation software and facilities.

Conflict of interest

The authors declare that there is no interests in this paper.

References

1. Liang GZ, Chen FC (2020) A compact dual-wideband bandpass filter based on open-/short-circuited stubs. *IEEE Access* 8: 20488–20492. https://doi.org/10.1109/ACCESS.2020.2968518
2. Liu S, Xu J, Xu ZT (2016) Compact dual-band bandpass filters using complementary split-ring resonators with closely spaced passbands. *Electron Lett* 52: 1312–1314. https://doi.org/10.1049/el.2016.1176
3. Li D, Wang JA, Liu Y, Chen Z (2019) Miniaturized dual-band bandpass filter with sharp roll-off using ring-loaded resonator. *IEEE Access* 8: 25588–25595. https://doi.org/10.1109/ACCESS.2019.2958390
4. Zhang Z, Xia M, Li G (2022) Compact Dual-Band Bandpass Filter with High Selectivity Using Stub-Loaded Stepped-Impedance Resonators. *Progress in Electromagnetics Research Letters* 102: 101–107. https://doi.org/10.2528/PIERL21112501
5. Zhou K, Zhou CX, Wu W (2018) Dual-mode characteristics of half-mode SIW rectangular cavity and applications to dual-band filters with widely separated passbands. *IEEE T Microw Theory* 66: 4820–4829. https://doi.org/10.1109/TMTT.2018.2865557
6. Zhou K, Zhou CX, Wu W (2017) Substrate-integrated waveguide dual-mode dual-band bandpass filters with widely controllable bandwidth ratios. *IEEE T Microw Theory* 65: 3801–3812. https://doi.org/10.1109/TMTT.2017.2694827
7. Wang X, Wang J, Zhu L, Choi WW, Wu W (2019) Compact stripline dual-band bandpass filters with controllable frequency ratio and high selectivity based on self-coupled resonator. *IEEE T Microw Theory* 68: 102–110. https://doi.org/10.1109/TMTT.2019.2945768
8. Khani S, Danaie M, Rezaei P (2019) Miniaturized microstrip dual-band bandpass filter with wide upper stop-band bandwidth. *Analog Integrated Circuits and Signal Processing* 98: 367–376. https://doi.org/10.1007/s10470-018-1254-x
9. Dong X, Li M, Li Y, Da Xu K (2016) Dual-band bandpass filters using open-/short-circuited stub-loaded quarter-wavelength resonators. *2016 IEEE MTT-S International Microwave Workshop Series on Advanced Materials and Processes for RF and THz Applications (IMWS-AMP)*, 1–3. https://doi.org/10.1109/IMWS-AMP.2016.7588392
10. Deng K, Chen Z, Hu G, Feng W (2019) Dual-band bandpass filters with multiple transmission zeros using $\lambda/4$ stepped-impedance resonators. *International Journal of RF and Microwave Computer-Aided Engineering* 29: e21469. https://doi.org/10.1002/mmce.21469
11. Peng Y, Zhang L, Fu J, Wang Y, Leng Y (2015) Compact dual-band bandpass filter using coupled lines multimode resonator. *IEEE Microwave and Wireless Components Letters* 25: 235–237. https://doi.org/10.1109/LMWC.2015.2400936
12. Huang W, Li L, Li L, Dong J (2020) A compact CPW bandpass filter based on spiral-shaped DGSs for 5G frequency band. *Prog Electrom Res Lett* 94: 27–34. https://doi.org/10.2528/PIERL20072403

13. Liu C, Deng Z, Liu X, Luo X (2019) A Wideband Bandpass Filter with Broad Stopband and Ultra-Wide Reflectionless Range for 5G Applications. *In 2019 IEEE MTT-S International Microwave Symposium (IMS)*, 834–837. https://doi.org/10.1109/MWSYM.2019.8700856
14. Praveena N, Gunavathi N (2023) High Selectivity SIW Cavity Bandpass Filter Loaded CSRR with Perturbing Vias for Sub-6 GHz Applications. *PIER Letters* 109: 103–110. https://doi.org/10.2528/PIERL22122008
15. Riaz M, Virdee BS, Shukla P, Ouazzane K, Onadim M (2020) Quasi-elliptic dual-band planar BPF with high-selectivity and high inter-band isolation for 5G communications systems. *Microw Opt Technol Lett* 62: 1509–1515. https://doi.org/10.1002/mop.32197
16. Xu Z, Wu Y, Dong Q, Wang W (2022) Miniaturized Dual-Band Filter Using Dual-Mode Dielectric Waveguide Resonator. *IEEE Microwave and Wireless Components Letters* 32: 1411–1414. https://doi.org/10.1109/LMWC.2022.3193424
17. Zhang Y, Ma K, Chen X (2022) A compact low-cost dual-band bandpass filter with enhanced suppression using substrate integrates suspended line technology. *Microw Opt Tech Lett* 64: 276–282. https://doi.org/10.1002/mop.33100
18. Boufouss R, Najid A (2021) High Selectivity Dual-Band Bandpass Filter for 5G Mobile Communications, *In 2021 4th International Conference on Advanced Communication Technologies and Networking (CommNet)*, 1–5. https://doi.org/10.1109/CommNet52204.2021.9642020
19. Wada K, Awai I (1999) Heuristic models of half-wavelength resonator bandpass filter with attenuation poles. *Electron Lett* 35: 401–402. https://doi.org/10.1049/el:19990207
20. Hong J-SG, Lancaster MJ (2004) *Microstrip filters for RF/microwave applications*. Hoboken, N.J, Wiley,
21. Zhang H, Ma K, Zhang W, Yan N (2023) A novel self-packaged DBBPF with multiple TZs for 5G sub-6 GHz applications. *Microw Opt Tech Lett* 65: 62–68. https://doi.org/10.1002/mop.33455
22. Tharani D, Barik RK, Cheng QS, Selvajyothi K, Karthikeyan SS (2021) Compact dual-band SIW filters loaded with double ring D-shaped resonators for sub-6 GHz applications. *J Electromagnet Wave* 35: 923–936. https://doi.org/10.1080/09205071.2020.1865211
23. Zhang W, Ma K, Zhang H, Fu H (2020) Design of a Compact SISL BPF With SEMCP for 5G Sub-6 GHz Bands. *IEEE Microwave and Wireless Components Letters* 30: 1121–1124. https://doi.org/10.1109/LMWC.2020.3030189
24. Hsu W-L, Lyu P-Y, Chang S-F (2020) Design of a miniature dual-band bandpass filter with interlocked stepped-impedance resonators for 5G new radio access technology. *Int J Microw Wireless Technol* 12: 733–737. https://doi.org/10.1017/S1759078720001026
25. Hou Z, Liu C, Zhang B, Song R, Wu Z, Zhang J, et al. (2020) Dual-/Tri-wideband bandpass filter with high selectivity and adjustable passband for 5G mid-band mobile communications. *Electronics* 9: 205. https://doi.org/10.3390/electronics9020205

AIMS Press